Journal of Electroanalytical Chemistry xxx (2010) xxx–xxx

Contents lists available at ScienceDirect

Journal of Electroanalytical Chemistry

journal homepage: www.elsevier.com/locate/jelechem

PM IRRAS spectroelectrochemistry of layer-by-layer self-assembled polyelectrolyte multilayers

Mario Tagliazucchi [a], Lucila P. Méndez De Leo [a], Alejandro Cadranel [a], Luis M. Baraldo [a], Edgar Völker [a], Cecilia Bonazzola [a], Ernesto J. Calvo [a,*], Vlad Zamlynny [b]

[a] INQUIMAE, Departamento de Química Inorgánica, Analítica y Química Física, Facultad de Ciencias Exactas y Naturales, Universidad de Buenos Aires, Argentina
[b] Chemistry Department, Acadia University, 6 University Avenue, Wolfville, Nova Scotia B4P 2R6, Canada

ARTICLE INFO

Article history:
Received 5 November 2009
Received in revised form 29 January 2010
Accepted 8 February 2010
Available online xxxx

Article in honour of Jacek Lipkowski on the occasion of his 65th birthday.

Keywords:
Infrared spectroscopy
PM IRRAS
Polyelectrolyte multilayer
Redox polymer
Pentacyanoosmate
Ion exchange

ABSTRACT

In situ polarization modulation infrared reflection absorption spectroscopy (PM IRRAS) has been used to study layer-by-layer self-assembled films made of a novel redox polymer bearing an osmium pentacyano pyridine complex (PAH-OsCN) and polyacrylic acid at different electrode potentials and solution compositions. PM IRRAS provides information on the oxidation state of the osmium complex, the fraction of protonated carboxylates and the content of IR-active counterions (such as nitrate) as well as water content (hydratation of the multilayer). It has an advantage over SNIFTIRS because it measures the absolute IR-signal arising from the molecular species at the interface rather than its variation with respect to a reference state. For instance, we show that only a fraction of the total number of redox sites responds to changes in the electrode potential as expected from the Nernst equation. The remaining sites are trapped in the Os(II) or Os(III) states and can only be oxidized/reduced by chemical agents in solution. We also present spectroscopic evidence that nitrate ions enter into the film during oxidation and leave during reduction. The number of these anions involved in the first process is larger than that participating in the latter and hence nitrate accumulates within the film. This finding is analyzed in terms of two possible mechanisms.

1. Introduction

In situ infrared vibrational spectroscopies are valuable tools to study single and multiple molecular layers at interfaces. These techniques allow detecting, identifying and quantifying the interfacial species and convey information on their orientation and local environment. The most widely used techniques are attenuated total internal reflection (ATR) spectroscopy [1] and the reflection–absorption spectroscopies based on the modulation of the electrode potential (subtractively normalized interfacial Fourier transform infrared spectroscopy, SNIFTIRS) and the polarization of the incident beam (polarization modulation infrared reflection absorption spectroscopy, PM IRRAS) [2]. In SNIFTIRS a reference spectrum is measured for a given electrode potential and then another spectrum is measured at a different potential. A difference between these spectra normalized by the reference spectrum is a SNIFTIRS spectrum proportional to absorbance of infrared light due to surface species. The creation or destruction of surface species gives raise to negative or positive bands, respectively. In PM IRRAS, the polarization of the incident radiation is modulated between orthogonal components in the plane of incidence (p) and out of the plane of incidence (s) [2,3]. The electric field of the p-polarized beam is enhanced at the metal surface while the s-polarized beam almost vanishes and therefore is insensitive to the presence of the species at the interface. By using the s-polarized component as the background and the p-polarized component as the signal, PM IRRAS can directly measure the absolute absorbance of the molecules at the surface (i.e. absorbance which is not dependent on the reference state like in the case of SNIFTIRS). PM IRRAS has been successfully employed to measure the spectra of self-assembled monolayers and Langmuir Blodgett films by Lipkowski's research group [4–8], who were the first to use PM IRRAS for quantitative in situ investigation of adsorption of insoluble surfactants at charged metal surfaces. Lipkowski's group has significantly advanced in the understanding of the influence of the electric field on biomimetic systems, such as phospholipids monolayers and bilayers as well as important biomembrane constituents like cholesterol and membrane polypeptides.

Polyelectrolyte films obtained by layer via layer-by-layer (LbL) deposition are widely studied because of their potential technological applications and due to the interesting fundamental questions that arise from their complex nature [9]. Long range electrostatic forces, ion pairing, hydrophobic interactions, chemical equilibria

* Corresponding author. Tel.: +54 11 4576 3378; fax: +54 11 4576 3341.
E-mail address: calvo@qi.fcen.uba.ar (E.J. Calvo).

1572-6657/$ - see front matter © 2010 Elsevier B.V. All rights reserved.
doi:10.1016/j.jelechem.2010.02.013

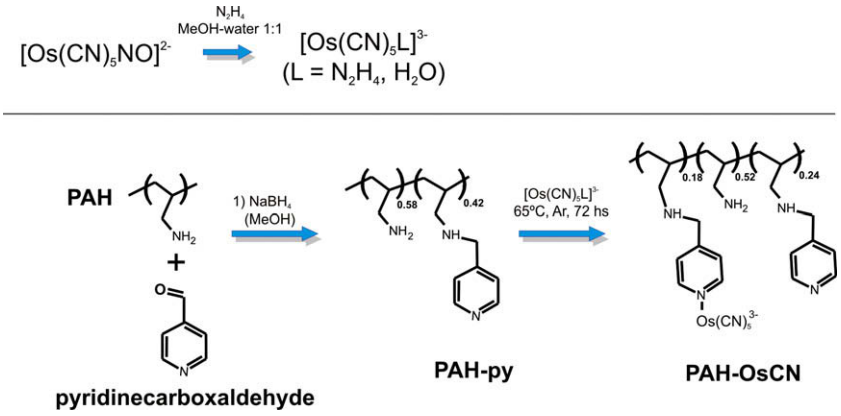

Fig. 1. Synthetic strategy for PAH-OsCN.

and osmotic forces among other factors determine the structure and composition of the resulting coatings. LbL multilayers are not in a true equilibrium state because their internal organization is determined by the interdiffusion of the polyelectrolytes, that can be limited to a very few layers or span across the entire film (exponential growing regime). As a consequence, dynamics in LbL multilayers span over several different timescales, the history of the film is important and its properties often exhibit hysteresis upon cycling of external conditions [10,11].

Important insights about the presence of ions and water within these complex systems have been obtained by Schlenoff and coworkers using ATR-FTIR (attenuated total internal reflectance Fourier transform infrared spectroscopy). The authors have shown that the perchlorate content in an LbL film increases linearly with the $NaClO_4$ activity in solution due to the rupture of intrinsic polyion—polyion bonds to form extrinsic polyion-ion pairs (doping with salt) [12,13]. In a related study, the internal hydration of multilayers and the doping level were simultaneously measured in solutions of different anions [14]. This study showed that less hydrated ions are better dopants, revealing a relationship between hydrophobic forces and polyion–polyion association in polyelectrolyte multilayers. Infrared spectroscopy has also been used to study the state of protonation of weak acid–base groups within LbL films. For example Rubner and co-workers used ex-situ FTIR spectroscopy to probe the degree of ionization of polyacrylic acid (PAA) assembled with different polycations as a function of adsorption pH [15]. Xie and Granick employed ATR-FTIR to follow the degree of ionization of a single layer of a poly(carboxylic) acid during the LbL assembly of a strong polycation and a strong polyanion on its topmost layer [16,17]. They showed that the carboxylate groups experienced deprotonation (protonation) during the assembly of the strong polyacid (polybase), an interesting example that points out the complexity of interactions in LbL films.

Multilayer films made of redox active polyelectrolytes [18] exhibit an additional level of complexity to that described above due to the presence of a redox couple that can exist either in a reduced or in an oxidized state. Changes in the oxidation state of the redox couple alters the charge balance within the film. This process triggers counterion [19,20] and solvent fluxes [11,21,22] and can produce changes in the protonation state of weak acid–base groups [23]. Multilayer films made of PAH-Os, a polyallylamine derivatized with the complex $[Os(bpy)_2ClpyX]^{+/2+}$ (bpy: bipyridine, pyX: substituted pyridine attached to the polymer backbone), have been extensively studied with electrochemical quartz crystal microbalance (EQCM) [11,22], probe beam deflection [19] (PBD) and SNIFTIRS [21,22,24]. The SNIFTIRS spectrum for the oxidation of Os(II) in $(PAH\text{-}Os/PVS)_{11}$ (PVS: poly(vinyl sulfonate)) multilayers showed small dipolar bands in the pyridine and sulfonate regions ascribed to the effect of the oxidation state of the complex in the vibrational frequencies of these groups and a positive band at the H_2O bending frequency associated with water influx [21,22,24].

While SNIFTIRS was especially useful to provide simultaneous and chemically specific information about several molecular species in PAH-Os/polyanion multilayers, it suffers from some important limitations. Its differential nature is a major drawback because the technique measures changes in the absorbance of the species rather than their absolute values. Furthermore the signal from the bulk solution for the experimental conditions of interest should exactly match the signal in the reference state. The spectra of interest and the reference must therefore be acquired without changes in the thickness of the aqueous electrolyte cavity or the concentration of IR-active species in solution. As a consequence, it is difficult to study the effect of varying bathing solution composition (added electrolytes or pH) on the inner properties of the film. Finally, the redox complex attached to the polymer used in previous experiments ($[Os(bpy)_2ClpyX]^{+/2+}$) has very weak bands in the pyridine region that do not undergo significant changes with the oxidation state of the metal and that overlaps with other peaks in the spectrum.

In this publication we overcome the limitations of previous SNIFTIRS studies by using PM IRRAS spectroscopy in combination with a novel IR-active redox polymer, PAH-OsCN: a polyallylamine derivatized with the IR-active group $[Os(CN)_5pyX]^{3-/2-}$ (where pyX represents a modified pyridine covalently tethered to the polymer backbone, see polymer structure in Fig. 1). The CN bond in the pentacyano redox couple presents different and well defined stretching bands in its reduced and oxidized forms in contrast to the small shifts observed for the pyridine and bipyridine units in PAH-Os. We will show the use of PM IRRAS spectroscopy to determine the oxidation state of a PAH-OsCN/PAA multilayer as well as the protonation and hydration states and the content of mobile ions.

2. Experimental section

Chemicals and solutions. 3-mercapto-1-propanesulfonic acid sodium salt, MPS (Aldrich), poly(acrylic acid) sodium salt, PAA (Aldrich, 35% in water Mw 100,000), poly(allylamine) chloride salt, PAH (Aldrich Mw 56,000) and D_2O (Aldrich, 99.9%) were used as supplied. Other reagents were analytical grade and were used without further purification. Polyelectrolyte solutions were prepared with 18 MΩ cm Milli-Q (Millipore) deionized water and their pH was adjusted to pH 7 (PAH-OsCN) or pH 4 (PAA) using either HCl or NaOH 0.1 M. The polyelectrolyte concentrations were 10 mM for PAA and 2 mM for PAH-OsCN (determined from the

UV–vis spectrum of working solution and the ε_{MLCT} $[Os(CN)_5pyX]^{3-}$ = 5460 M^{-1} cm^{-1} [25]).

Synthesis of polymer PAH-py. The pyridine modified poly(allylamine) (PAH-py) used in the synthesis of PAH-OsCN, was prepared from PAH and pyridinecarboxaldehyde by reductive amination [26]. The aldehyde (0.12 ml, 1.1 mmol) was added dropwise to a solution of 300 mg of PAH (3.24 mmol) and 0.5 ml of triethylamine (TEA) in 15 ml of anhydrous methanol. The reaction mixture was ice-cooled and stirred for 3 h and an excess of $NaBH_4$ was added in small portions within one hour. After one additional hour, methanol was removed by vacuum evaporation and the solid product was washed with sulfuric ether, dissolved in HCl acidified water and purified by ultrafiltration. The solution was freeze–dried and the final product was analyzed by ^1H NMR and FTIR.

Synthesis of PAH-OsCN. The complex $K_2[Os(CN)_5NO]\cdot H_2O$, prepared and purified according to the literature [25,27,28], was mixed (40 mg) at room temperature with N_2H_4 (20 μl) in 5 ml of deionized water–methanol 1:1. The disappearance of NO was monitored by following the decay of the $[Os(CN)_5NO]^{2-}$ UV absorption band at 420 nm. PAH-py (40 mg) dissolved in water–methanol 1:1 and 50 μl of TEA were added to the reaction mixture after 24 h. The reaction was continued for 3 days at 65 °C under Ar atmosphere. The complex-substituted polymer precipitated during this step. It was dissolved by acidification with HNO_3 and the as obtained solution was dialyzed against NaCl 0.5 M + HNO_3 1 mM for 2 days and finally against Milli-Q water for 5 days. The final product was analyzed by UV-vis spectroscopy in solution (Shimadzu UV-1603 spectrophotometer), FTIR spectroscopy in KBr pellet (Thermo Nicolet 8700) and XPS spectroscopy of a dried-casted film (Specs SAGE 150). The substitution degree was estimated from the Os/N ratio determined from the N 1s and Os 4f XPS peaks (0.078) [29] and the ratio of pyridine units to allylamine segments in PAH-py (0.42), measured by integration of aromatic and aliphatic H in ^1H NMR. This calculation yields a ratio of allylamine:allylamine-py:allylamine-$[pyOs(CN)_5]^{3-/2-}$ of 58:24:18 (see Fig. 1). Since the freeze dried solid was insoluble in any available deuterated solvent ($CDCl_3$, d^6-DMSO, D_2O or D_2O + CF_3COOH), ^1H NMR for PAH-OsCN was not performed.

PM IRRAS experiments. The polarization modulation infrared reflection absorption spectroscopy (PM IRRAS) experiments were performed at the University of Buenos Aires, on a Thermo Nicolet 8700 (Nicolet, Madison, WI) spectrometer equipped with a custom made external tabletop optical mount, a MCT-A detector (Nicolet), a photoelastic modulator (PEM) (PM-90 with a II/Zs50 ZnSe 50 kHz optical head, Hinds Instruments, Hillsboro, OR), and a Synchronous Sampling Demodulator (GWC Instruments, Madison, WI). A custom made Teflon® electrochemical cell was coupled to the set-up to acquire in situ IR spectra. The working electrode was a polycrystalline gold disc. The IR window was a 1 in. (~25 mm) CaF_2 equilateral prism (Harrick Scientific Technology, PleasantVille, NY). Prior to the assembly of the spectroelectrochemical cell, the gold electrode was modified with the LbL film as detailed (see below). The cell was filled with a saline solution using deuterated water as solvent, as detailed later.

The IR spectra were acquired with the PEM set for a half wave retardation at 1700 cm^{-1}. The angle of incidence was set to 55°, which gives the maximum of mean squared electric field strength at the metal surface for the CaF_2/D_2O/gold cell. The thickness of the thin layer of electrolyte between the optical window and the gold electrode was typically set to 3 μm and was determined by comparing the experimental reflectivity spectrum of the thin layer cell attenuated by the layer of the solvent, to the reflectivity curve calculated from the optical constants of the cell constituents [2,8]. The demodulation technique developed in Corn's laboratory was used in this work. The absorbance of surface confined species in PM IRRAS spectra is given by

$$\Delta S(v) = \frac{2|I_s - I_p|}{(I_s + I_p)} \quad (1)$$

where I_s and I_p are the intensities of s- and p-polarized light arriving on a detector.

A modified version of a method described by Buffeteau et al. [30] was used to correct the spectra for the PEM response. These corrections were performed using PEM functions measured for identical conditions to those used for spectral acquisition. Baseline correction was performed by lineal interpolation between the data points corresponding to the minima on both sides of each peak (the wavelengths of these minima were within a few cm^{-1} for all the spectra).

The electrochemical cell was a conventional three-electrode cell connected to a Jaissle IMP88 Potentiostat (Germany) controlled by a homemade PM IRRAS acquisition software via a digital to analog converter (Agilent USB AD/DA converter). All potentials were measured and reported with respect to a Ag/AgCl (KCl 3 M) reference electrode. The electrode potential was varied from 0.35 V to 0.75 V and back to 0.35 V using 0.050 V steps. Each potential step comprises an equilibration time of 120 s followed by the acquisition of the spectrum by averaging of 200 scans at 4 cm^{-1} resolution.

Electrode preparation. The PM IRRAS gold electrode was mirror polished with alumina 1 μm, 0.3 μm and 0.05 μm and cleaned by sonication in isopropanol, isopropanol: Milli-Q water and Milli-Q water. Before thiol adsorption, the electrode was cleaned by potential cycling between 0 and 1.6 V in 2 M H_2SO_4 at 10 V s^{-1}, followed by a scan at 0.1 V s^{-1} to ensure surface cleanness. The electrochemically active area was estimated from the gold oxide reduction peak [31].

Before layer-by-layer coating, gold electrode surfaces were negatively charged by adsorption of MPS for 30 min in H_2SO_4 10 mM. Polyelectrolytes were assembled by alternated immersion in PAH-OsCN and PAA solutions for 15 min (starting with PAH-OsCN solution) and thoroughly rinsed with water. This procedure was repeated until the desired number of layers was achieved.

Ellipsometry. Film thickness was determined from ellipsometric experiments performed with a variable angle rotating analyzer automatic ellipsometer (SE 400 model, Sentech GmbH, Germany) equipped with a 632.8 nm laser as polarized light source. All measurements were performed at an incidence angle of 70.00°. After each adsorption step, the sample was rinsed with Milli-Q water and dried with N_2 and the ellipsometric parameters (ψ and Δ) were collected manually. All adsorption, rising and drying steps were carried out avoiding any variations of the electrode position in order to keep the system alignment. The ellipsometric angles were fitted with a three-layer model (air/polymer film/substrate [32]).

3. Results and discussion

3.1. Synthetic strategies and characterization of the novel redox polymer PAH-OsCN

Fig. 1 shows the synthetic strategy for the IR-active redox polymer, PAH-OsCN. This strategy is based on exchanging a labile ligand L in the complex $Os[(CN)_5pyX]^{3-}$ by the pyridine units in a modified polyallylamine (PAH-py). Infrared transmission spectroscopy in KBr pellets have been used to follow the synthesis (Fig. 2A and 2B). The spectrum of PAH-py shows a small band at 3060 cm^{-1} and several bands in the range 1600–1200 cm^{-1} (i.e. the band at 1414 cm^{-1}) that can be assigned to pyridine aromatic C—H stretching mode and ring stretching vibrations, respectively [24]. A very intense band at 2034 cm^{-1} appears after introduction of the $-Os(CN)_5^{3-}$ group (see PAH-OsCN spectrum) that corresponds to

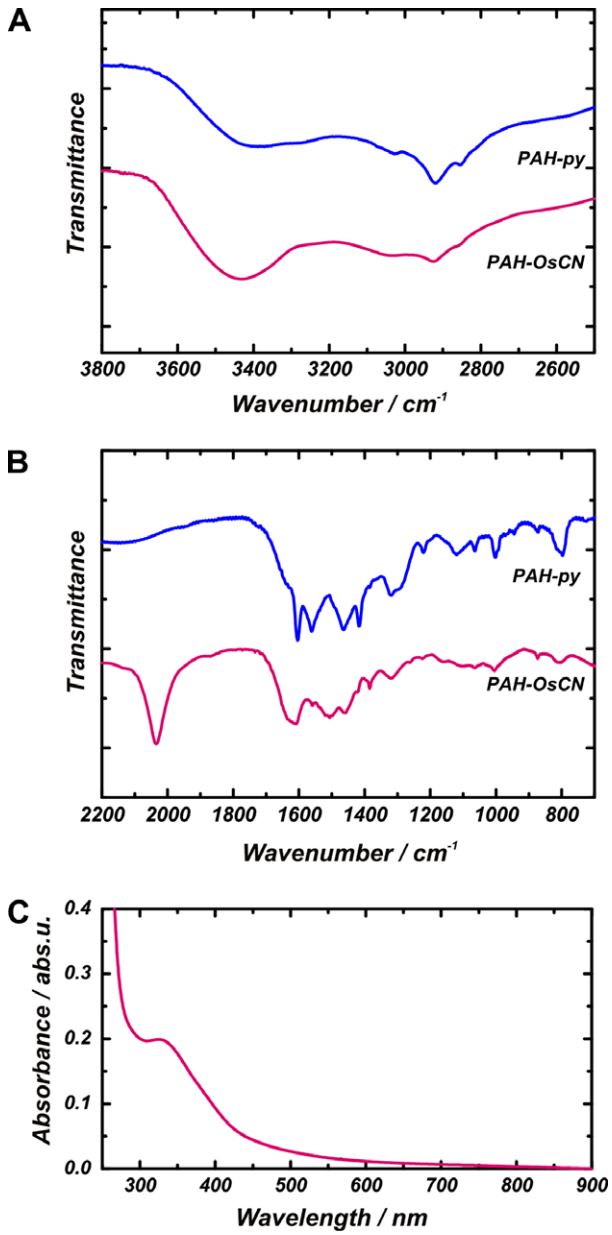

Fig. 2. Transmittance FTIR spectra in KBr pellet for PAH-py and PAH-OsCN in the 3800–2600 cm^{-1} (A) and 2200–700 cm^{-1} (B) regions. UV–vis spectra for a PAH-OsCN in solution (C).

the C≡N stretching mode in the reduced redox couple (see below). Pyridine bands for PAH-OsCN are less resolved than for PAH-py probably because in this polymer there are two different types of pyridine units (those that are modified with the complex and those that are not).

The UV–vis spectra of PAH-OsCN (Fig. 2C) shows the metal to ligand charge transfer (MLCT) band at 324 nm, close to the literature value for the complex $[Os(CN)_5py]^{3-}$, λ_{MLCT} = 318 nm [25]. The lack of absorption in the red and near-IR regions suggests the absence of polynuclear mixed valence Os complexes. Even though the $[(NC)_5Os^{II}(\mu\text{-}CN)Os^{III}CN_5]^{6-}$ has not been characterized, its ruthenium analogue has a broad band at 1100 nm [33].

To our best knowledge, redox polymers bearing the $[Os(CN)_5pyX]^{3-/2-}$ couple have not been previously reported. Redox polymers based on $[Fe(CN)_5pyX]^{3-/2-}$ have been prepared [26,34], however their application in polyelectrolyte modified electrodes can be limited by their fast kinetics of ligand exchange. For instance, the rate constants for the dissociation of the pyridine ligand in $[M(CN)_5py]^{3-/2-}$ in aqueous solutions are $6.1.10^{-2}$ s^{-1} ($\tau_{1/2}$ = 11 s) for M=Fe and 2.7. 10^{-7} s^{-1} ($\tau_{1/2}$ = 30 days) for M=Os [28]. Even though the stability of polymers modified with $[M(CN)_5pyX]^{3-/2-}$ complexes have not been studied, the relative stability constants of the pyridine complexes suggests that electroactive films based on the osmium pentacyano group would be more kinetically stable than their iron based counterparts.

3.2. Electrochemical response and film thickness of PAH-OsCN polyelectrolyte multilayers

Since it was previously shown that polyanion capped multilayers exhibit a hindrance for the redox process [35] this work considers only films finished in PAH-OsCN. Fig. 3A shows the cyclic voltammograms in 50 mM NaF for PAH-OsCN/PAA films with different number of layers. The figure shows that the area of the redox peak increases with the number of layers. The multilayers bearing 0.5 and 1.5 PAH-OsCN/PAA bilayers present symmetrical oxidation and reduction current–potential waves. The peak separation increases from 6–18 mV for these films to 25 and 54 mV for the films bearing 2.5 and 3.5 bilayers suggesting the transition from thin layer behavior to a diffusion controlled regime due to the increase in thickness [36].

The average peak potential for the current–potential curves in Fig. 3A is 0.539 V. This peak potential is affected by the presence

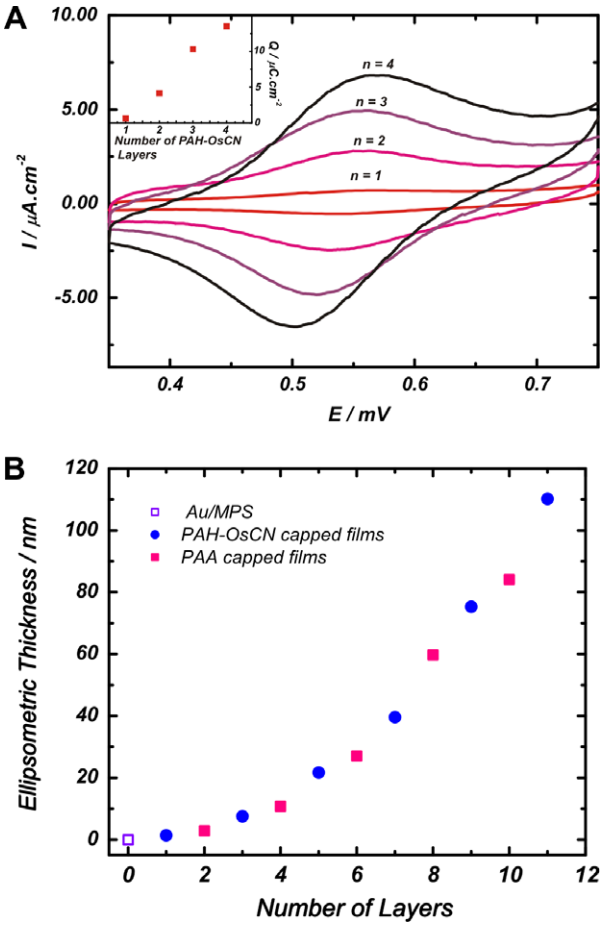

Fig. 3. A. Voltammograms for a Au/MPS/(PAH-OsCN/PAA)$_{n-1}$PAH-OsCN electrode in NaF 50 mM. Scan rate: 50 mV/s. Inset: average peak charge vs. *n* (number of PAH-OsCN layers). B. Ellipsometric film thickness as a function of the number of dipping cycles in PAH-OsCN and PAA solutions.

of the Donnan potential at the interface [29,37]. We measured an average peak potential of 0.464 V in high ionic strength solutions (KNO_3 2 M) where the interfacial potential vanishes. The latter value can be considered very close to the standard redox potential of the couple and it is similar to the value of E^0 = 0.44 reported for the $[Os(CN)_5py]^{3-}$ complex in solution [25]. Since the apparent potential decreases when increasing the ionic strength, the Donnan potential is positive and the films in Fig. 3A must be anionic exchangers. These observations are in good agreement with the set of rules proposed in Ref. [29] to determine the sign of the Donnan potential in LbL films based on the charge of the outmost layer and the relationship between the assembly and testing pHs. In this case, the assembly pH is similar to the testing pH and thus the positive outmost layer defines the sign of the Donnan potential.

Fig. 3B shows the ellipsometric thickness of PAH-OsCN/PAA multilayers as a function of the number of dipping steps. As previously noted for PAH-Os/PVS [29] and many other LbL films, the thickness per layer is smaller for the first dipping cycles than for the following ones due to the effect of the substrate. From the current–potential waves in Fig. 3A that do not present charge transport limitations (films bearing 0.5, 1.5 and 2.5 bilayers) and the corresponding film thicknesses, we estimate the concentration of osmium sites that can be electrochemically addressed to be (50 ± 6) mM . This concentration is similar to those previously reported for PAH-Os/PVS [35] and PAH-Os/glucose oxidize [38] multilayers. As we discuss below based on in situ PM IRRAS evidence, the real concentration of osmium sites is actually larger than this value, since only a small fraction can be addressed by the electrode.

3.3. In situ PM IRRAS spectroscopy

Fig. 4 shows in situ PM IRRAS spectra for PAH-OsCN/PAA modified electrodes in HF/NaF buffer solutions in D_2O. The curves in the figure have been measured with (curve A) and without (curve B) added $NaNO_3$ and for pH 8 (curve C) and pH 4 (curve B) solutions. The figure displays two bands at 2050 and 2094 cm^{-1} due to the stretching vibration of the C≡N bond in the reduced Os(II) and oxidized Os(III) complexes, respectively (note that these spectra were recorded for an electrode potential of 0.60 V). This assignment is based on the frequencies of the CN stretching bands reported for the Os(II) complex $[Os(CN)_5py]^{3-}$ (2050 cm^{-1}) [25] and for the Os(III) complex $[Os(CN)_6]^{3-}$ (2080 cm^{-1}) [39]. Protonated amines in PAH present also a band in this region due to the combination of the NH_3^+ asymmetric deformation and torsional oscillation bands at 1580 cm^{-1} and 480 cm^{-1}, respectively [40]. This band is weaker than the CN stretching band and very broad (see spectra in Refs. [10,21]), therefore its contribution to the final spectra is mainly removed during baseline correction.

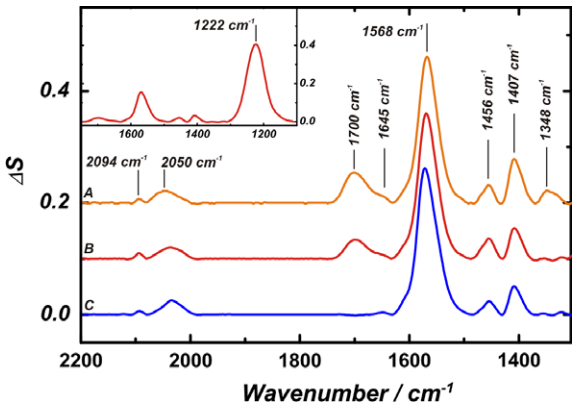

Fig. 4. In situ PM IRRAS spectra of a $(PAH\text{-}OsCN/PAA)_4PAH\text{-}OsCN$ film in A. 50 mM NaF/HF pH 4 + 50 mM $NaNO_3$ buffer, B. 50 mM NaF/HF pH 4 buffer, C. NaF 50 mM pH 8. The spectra were measured for an electrode potential of 0.6 V and normalized to have the same ΔS at 1568 cm^{-1}. The inset shows an extended wavenumber range of the spectrum in B for an extended wavenumber range that includes the D_2O deformation peak at 1222 cm^{-1}.

The spectra measured in acid conditions (curves A and B) show four bands in the 1700–1400 cm^{-1} region. Following references [15,41] they correspond to: (i) the CH_2 bending modes in PAH-OsCN and PAA at 1456 cm^{-1}, (ii) the asymmetric stretching band of carboxylate groups, $\nu_a(COO^-)$ = 1567 cm^{-1}, (iii) the symmetric stretching band of carboxylate groups, $\nu_s(COO^-)$ = 1407 cm^{-1} and (iv) the stretching of the C=O bond in the protonated carboxylic acids ν(COOH) = 1700 cm^{-1}. As expected, the latter peak is absent for the electrode immersed in basic solution (curve C). That spectrum shows also a very small peak at 1645 cm^{-1} (which appears as a small shoulder in spectra A and B) that probably arises from the asymmetric bending mode of NH_3^+ in PAH, expected at 1626 cm^{-1} [15]. We should mention that the redox polymer, PAH-OsCN, exhibits weak peaks in this region that overlaps the C=O PAA bands, such as those observed in Fig. 2B at 1561, 1507, 1465 and 1422 cm^{-1}. These peaks can be assigned to the asymmetric and symmetric deformations of NH_3^+ (expected at 1625–1560 and 1550–1505 cm^{-1}, respectively [40]) and the ring stretching modes for monosubstituted pyridines (expected at 1620–1570, 1580-1560, 1480–1450 and 1440–1415 cm^{-1} [24,40,42]).

The $\nu_a(COO^-)$ bands at 1567 cm^{-1} and the ν(COOH) bands at 1700 cm^{-1} can be used to estimate the extent of protonation of the carboxylates in PAA. Moreover, a rather straightforward comparison is possible because the extinction coefficients for these bands are very similar [16]. In the spectra A and B of Fig. 4, the $\nu_a(COO^-)$ band is more intense than the ν(COOH), which is unexpected considering the solution pH (4) and the pK_a for the carboxylic groups of PAA in solution (6.5) [15]. The experiment shows that, as it has been previously shown for many other LbL systems [15,17,43,44], there is a shift of the effective pK_a of polyelectrolytes embedded in these films that favors the ionized species (the apparent pK_a decreases for polyacids and increases for polybases). This effect is ascribed to the formation of polyion–polyion pairs.

Spectrum A shows a band at 1348 cm^{-1} that is absent in spectra B and C and that can be ascribed to the nitrate anions [45,46]. There is also a very intense band at 1222 cm^{-1} in all spectra (see inset in Fig. 4) that is assigned to the D_2O bending mode [45]. This band is equivalent to the H_2O bending mode band at 1648 cm^{-1} observed for in situ experiments in non-deuterated water solutions [22,45]. It should be noted that NO_3^- and D_2O are present not only inside the film but also in the bulk solution and therefore the bands at 1348 cm^{-1} and 1222 cm^{-1} have contributions from the free species in solution (the molecules that contribute to the PM IRRAS spectrum are those within a distance from the electrode comparable with a quarter of the measuring wavelength [2]). The rest of the bands in the spectra in Fig. 4 arise only from adsorbed species. We expect all species within the relatively thick multilayer to be randomly oriented and therefore changes in absorbance will be associated to changes in population rather than to changes in molecular orientation, as is usually done for PM IRRAS spectra of ultrathin Langmuir–Blodgett films or self-assembled monolayers [2,4–8,47–50].

Multilayer PAH-OsCN/PAA films are rather complex systems: In order to get a complete picture of the internal composition and charge balance within these films, the content of ions and water, the state of oxidation of the osmium complex and the state of protonation of the acid–base groups (amines and pyridines in PAH-OsCN and carboxylates in PAA) need to be determined. We have shown in this section that PM IRRAS provides information about all these variables except for the population of IR-silent ions (Na^+ and F^-) and the state of protonation of amino and pyridine groups in PAH-OsCN.

3.4. Spectroelectrochemistry of the $[Os(CN)_5pyX]^{3-/2-}$ group

The evolution of the CN—Os(II) and CN—Os(III) bands with increasing electrode potentials is shown in Fig. 5. It is apparent that the extinction coefficient for the CN band of the oxidized complex is lower than that of the reduced species, in agreement with previous observations for $[Fe(CN)_6]^{4-/3-}$ [51,52]. The formal redox potential for the redox couple is expected to be between 0.40 and 0.55 V for this electrode (depending on solution ionic strength) and therefore the lower and upper limits of the electrode potential shown in Fig. 5 (0.35 and 0.75 V) must correspond to totally reduced and totally oxidized films, respectively. However, the figure shows that this is not the case: an intense CN—Os(II) band is present even for $E = 0.75$ V. We have found that the CN—Os(II) band does not disappear even when holding the electrode potential at 0.75 V for 90 min, showing that the oxidation of osmium sites is not limited by the diffusion of redox charge.

Fig. 6 depicts the study of the chemical oxidation and reduction of the osmium sites in the multilayer with ex-situ PM IRRAS. The spectrum of the freshly prepared film exhibits only the CN stretching band corresponding to the reduced complex. Upon treatment with Ce(IV) in H_2SO_4 0.5 M ($E^\circ = 1.51$ V) for a few seconds and drying with N_2, the CN—Os(II) peak completely vanishes and the CN—Os(III) band appears in the spectrum. The process can be fully reverted by chemical reduction with ascorbic acid ($E^\circ = 0.18$ V). These results suggest that the failure to totally electro-oxidize the redox complexes in the film described in Fig. 5 occurs because there are some redox sites in the film that cannot be electrically addressed.

Fig. 7 shows the areas under the peaks for the CN—Os(II) and CN—Os(III) bands measured by in situ PM IRRAS as a function of electrode potential during three consecutive oxidation–reduction cycles. For each cycle the potential was increased from 0.35 V to 0.75 V in steps of 50 mV and then decreased back to 0.35 V in the same manner. The figure demonstrates that the peak areas for the first oxidation–reduction cycles are slightly larger than those for the following two cycles, probably due some potentially driven loss of loosely bound polymeric material. Note however that after this initial effect, there is no further decay in the CN signals (this is also observed for experiments with even more oxidation/reduction cycles than those shown in Fig. 7, see below) and that therefore the leaching of the osmium complex to the solution can be taken as negligible.

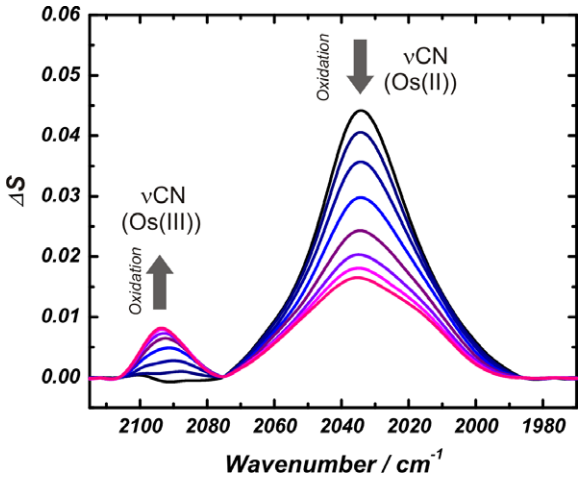

Fig. 5. In situ PM IRRAS spectra of a $(PAH\text{-}OsCN/PAA)_4PAH\text{-}OsCN$ film in 50 mM NaF for increasing electrode potentials (in the direction of the arrow): 0.40, 0.45, 0.50, 0.55, 0.60, 0.65, 0.70 and 0.75 V.

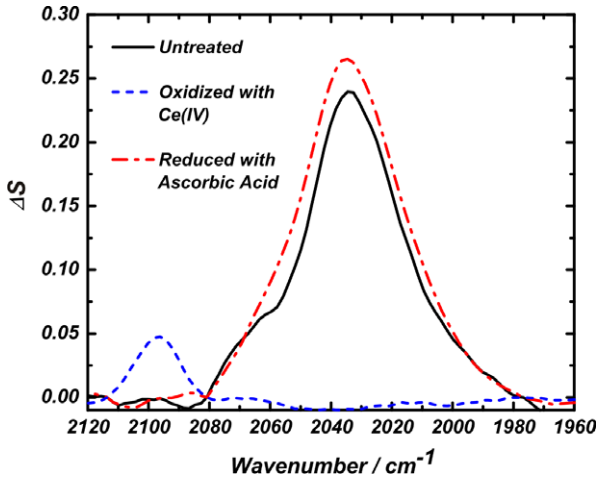

Fig. 6. Ex-situ PM IRRAS spectra of a freshly prepared $(PAH\text{-}OsCN/PAA)_4PAH\text{-}OsCN$ film (solid line) and after treatment with 0.1 M Ce(IV) in H_2SO_4 0.5 M (dashed line) and 0.1 M ascorbic acid (dash dotted line).

Although we have shown that some sites in the film cannot be electrochemically switched, we expect the rest to follow the Nernst equation for the $[Os(CN)_5pyX]^{3-/2-}$ couple. Under that condition, the areas of the CN—Os(II) and CN—Os(III) bands should be given by:

$$A_{CN-Os(II)} = A^0_{CN-Os(II)}\left[f_{CN-Os(II/III)}\left(\frac{\theta}{\theta+1}\right) + f^0_{CN-Os(II)}\right] \quad (2)$$

$$A_{CN-Os(III)} = A^0_{CN-Os(III)}\left[f_{CN-Os(II/III)}\left(\frac{1}{\theta+1}\right) + f^0_{CN-Os(III)}\right] \quad (3)$$

In these equations $f_{CN-Os(II/III)}$ is the fraction of the total osmium sites that can be electrochemically switched between Os(III) and Os(II) and $f^0_{CN-Os(II)}$ and $f^0_{CN-Os(III)}$ are the fractions of isolated redox sites trapped in the reduced and oxidized states, respectively. The sum of these three fractions is equal to one. The terms in parenthesis multiplying $f_{CN-Os(II/III)}$ in Eqs. (2) and (3) take into account the fraction of these sites that are oxidized or reduced according to the electrode potential, which determines θ:

$$\theta = \exp\left(-\frac{F(E - E^0_{app})}{RT}\right) \quad (4)$$

where E^0_{app} is the apparent potential of the $[Os(CN)_5pyX]^{3-/2-}$ couple. The areas of the CN—Os(II) and CN—Os(III) bands are therefore obtained in Eqs. (2) and (3) by multiplying the total fraction of reduced or oxidized osmium sites for a given electrode potential (terms in brackets) by the area of a totally reduced ($A^0_{CN-Os(II)}$) or totally oxidized film ($A^0_{CN-Os(III)}$), respectively.

The best fit curves to the data of the second and third oxidation–reduction cycles to Eqs. (2) and (3) are shown in Fig. 7 as solid lines. From the fit we get $f^0_{CN-Os(II)} = 0.34$, $f^0_{CN-Os(III)} = 0.09$, $f_{CN-Os(II/III)} = 0.57$, $(A^0_{CN-Os(II)}) = 0.98$, $(A^0_{CN-Os(III)}) = 0.11$ and $E^0_{app} = 0.545$ V. The best fit value for E^0_{app} is in good agreement with the average peak potential of 0.539 V observed in the experiments in Fig. 2. From the fraction of electrochemically addressable redox sites and their volumetric concentration (see above), we estimate the total concentration of osmium-pentacyano sites in the film to be (88 ± 10) mM.

Savéant has proposed that the transport of redox charge in polymer modified electrodes can be described as a percolation problem [53]. Electrically connected redox sites form clusters and complete oxidation/reduction of a cluster in electrical contact with the electrode will occur provided that the experimental timescale is larger than the timescale for electron-hopping. On the other

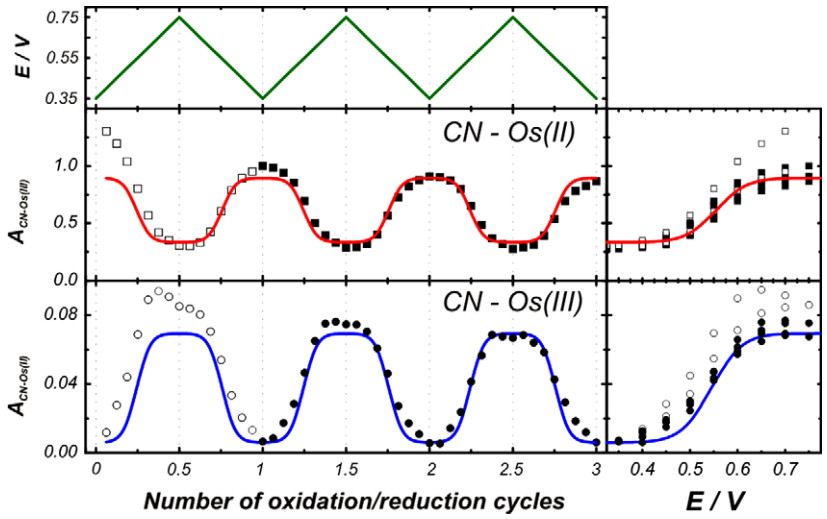

Fig. 7. Integrated peak areas of the CN–Os(II) and the CN–Os(III) IR-bands of a $(PAH\text{-}OsCN/PAA)_4PAH\text{-}OsCN$ electrode for three consecutive oxidation–reduction cycles (empty symbols: first cycle, solid symbols: last two cycles). Solid lines show the best fit of peak areas for the last two cycles to the Eqs. (2) and (3) (see main text). The upper panel shows the applied electrode potential. Right panels show the peak areas as a function of applied potential.

hand, a cluster that is not touching the electrode surface at any point cannot be electrically addressed. Polymer reorganization due to redox switching or to changes in electrolyte solution could reconfigure these clusters. For instance Hillman has referred to the electrical isolation of redox sites due to potential cycling as "charge trapping" and studied this processes in electrodeposited PVF films using EQCM [54].

In the case of redox polyelectrolyte multilayers, Anzai has claimed that the fractions of electrically addressable sites in PAH-Fc (polyallylamine modified with ferrocene) and PEI-Fc (poly(ethylenimine) modified with ferrocene) are in the range of 20–60% based on a comparison of the integrated CV charge and the total number of Fc sites estimated by QCM (Quartz Crystal Microbalance) [55] or UV–vis spectroscopy [56]. On the other hand, Schlenoff has proposed that all redox sites are oxidized/reduced in a poly(butanylviologen)/poly(styrenesulfonate) (PSS) multilayer film based on combined results from CV and UV–vis spectroscopy [57]. For a ferrocene polycation/PAA multilayer the combination of surface plasmon spectroscopy and CV measurements suggests that all the redox sites are in electrical contact with the electrode [58]. All these experiments are based on the comparison of results from two completely different experimental techniques reporting on the total and the electrochemically active number of sites. However, this indirect comparison is affected by the accuracy of some important parameters such as the density and stoichiometry of the polymers for QCM and the molar absorption coefficient inside the film for UV–vis measurements, as well as other sources of error like the determination of the electrochemically active area in CV measurements. The in situ spectro-electrochemical analysis with PM IRRAS allows a direct comparison of the population of oxidized and reduced sites and therefore it provides very reliable information about electrical connectivity inside the film. We should mention a related spectroelectrochemical experiment for PAH-Os/PVS films using Resonant Raman spectroscopy [59] that has shown a complete disappearance of the Os(II) resonant Raman signal after electrochemical oxidation.

3.5. Ion and solvent fluxes

In order to study ion exchange using IR techniques it is necessary that the supporting electrolyte solution contains an IR-active ion. Several anions have been used in the past for this purpose [14,52,60]: SCN^-, N_3^-, ClO_4^-, NO_3^-, $[Fe(CN)_6]^{4-/3-}$, $[Ni(CN)_4]^{2-}$, etc. We have chosen NO_3^- because its IR band does not overlap with any other intense band in the PAH-OsCN/PAA IR-spectrum (see Fig. 4) and because the electrochemical response of the film is not affected by this anion as it happens with more hydrophobic ions such as perchlorate [11]. Fig. 8 shows the nitrate band at 1348 cm^{-1} at increasing electrode potentials. This band corresponds to the doubly degenerated ν_3 vibration mode of the D_{3h} point symmetry group [45], which usually appears as a sharp peak in anhydrous crystals. In aqueous solution, the solvation of the anion with water molecules lowers the symmetry, the degeneration is removed and the band is split as observed in Fig. 8 [46].

Fig. 8 shows that the intensity of nitrate ν_3 band increases with the electrode potential indicating anion uptake during oxidation, in agreement with the anion exchange behavior expected from the sign of the Donnan potential for this film. Fig. 9A shows the integrated peak intensity for the nitrate and the CN—Os(III) bands recorded during four consecutive oxidation–reduction cycles. As expected, the maxima in nitrate content correspond to the maxima in the fraction of oxidized osmium sites. Fig. 9A also shows that the

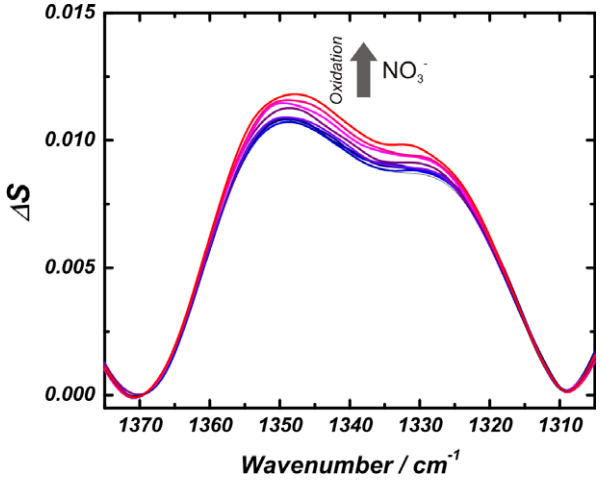

Fig. 8. In situ PM IRRAS spectra of a $(PAH\text{-}OsCN/PAA)_4PAH\text{-}OsCN$ film in NaF 50 mM and 10 mM $NaNO_3$ pH 8 solution for increasing electrode potentials (in the direction of the arrow): 0.35, 0.40, 0.45, 0.50, 0.55, 0.60, 0.65, 0.70 and 0.75 V.

intensity of nitrate band in the reduced state increases with the number of oxidation–reduction cycles. The plot of the nitrate peak area vs. the CN—OsCN(III) peak area in Fig. 9B presents hysteresis, showing that the number of nitrate ions that enter the film during oxidation is less than the number leaving during reduction. This interesting effect has been previously observed with other techniques. We will discuss it here in the light of the new information provided by PM IRRAS spectroscopy.

Ion fluxes in redox active polyelectrolyte multilayers have been first studied by Schlenoff using radioactive labeled $^{45}Ca^{2+}$ for cation exchanger multilayers made of poly(butylviologen) and PSS [20]. This experiment showed Ca^{2+} influx during reduction and Ca^{2+} release during oxidation. However, a monotonic increase in the Ca^{2+} content (for a given oxidation state of the film) with the number of redox cycles was observed. The effect has also been observed for a $(PAH\text{-}Os/PSS)_{14}PAH\text{-}Os$ electrode by EQCM [22]. The experiments showed an increase in electrode mass with the number of oxidation–reduction cycles which has been ascribed to the built-up of ions and solvent within the film. Probe beam deflection (PBD) has allowed direct observation of ion fluxes for this system [19]. This technique measures changes in the refractive index gradients in the solution adjacent to the electrode/electrolyte interface and thus provides information about ion fluxes instead of ion content [61]. Cation/anion fluxes measured by PBD showed that the film behaves as an anion exchanger. However, both the ionic and electronic transient currents decreased with the number of oxidation–reduction cycles showing a dynamical behavior in agreement with EQCM results. The experiment in Fig. 9 provides a spectroscopic proof of the intake of anions from solution which is in agreement with the previous experimental evidence.

The increase in the ionic content of multilayer films with the number of redox cycles points out the non-equilibrium nature of LbL. We can envisage two possible explanations. To analyze them, let us assume an anion exchanger polymer, pol-ox^n/pol-red^{n-1}. For the first oxidation cycle of a freshly prepared film we can write:

$$[\text{pol-red}^{n-1}]_{\text{film}} + A^-_{\text{aq}} \rightarrow [\text{pol-ox}^n A^-]_{\text{film}} + e^- \quad (5)$$

The first hypothesis to explain why some anions remain trapped in the film assumes that a fraction of the negative charge created during the reduction of the osmium couple is not compensated by anion release but by cation uptake. In other words, the reduction step can be described by:

$$[\text{pol-ox}^n A^-]_{\text{film}} + xC^+_{\text{aq}} + e^- \rightarrow x[\text{pol-red}^{n-1}A^-C^+]_{\text{film}} + (1-x)[\text{pol-red}^{n-1}]_{\text{film}} + (1-x)A^-_{\text{aq}} \quad (6)$$

This mechanism implies a decrease of permselectivity with the number of redox cycles.

An alternative mechanism considers that some sites in the oxidized film cannot be reduced, because they remain trapped in the oxidized state or because the timescale of the experiment is smaller than the characteristic timescale for electron-hopping diffusion. Once again, the amount of anions expelled during reduction is smaller to the amount taken up during oxidation:

$$[\text{pol-ox}^n A^-]_{\text{film}} + xe^- \rightarrow (1-x)[\text{pol-ox}^n A^-]_{\text{film}} + x[\text{pol-red}^{n-1}]_{\text{film}} + xA^-_{\text{aq}} \quad (7)$$

This mechanism is consistent with the decrease in electronic current observed in PBD experiments.

PM IRRAS has a major advantage over other techniques at the time of determining which mechanism is operative because it provides simultaneous and very specific information of the ion content and the state of film oxidation. Fig. 9A shows that the amount of Os(III) at the lower potential limit presents a small increase during the first redox cycle and then remains constant during the following oxidation–reduction cycles. Therefore the mechanism described by Eqs. (5) and (6) should be mainly responsible for the accumulation of counterions in the multilayer film under study.

Solvent uptake during oxidation and release during reduction has been proposed for $(PAH\text{-}Os/PSS)_{14}PAH\text{-}Os$ multilayers based on SNIFTIRS [21,22] measurements of the H_2O band at 1648 cm^{-1} and EQCM [11,22] experiments. For the PAH-OsCN/PAA system, we performed a similar analysis to that described in Fig. 9 for the D_2O band at 1222 cm^{-1}. This study showed that the intensity of this band does not change with the electrode potential. The difference between previous SNIFTIRS experiments for PAH-Os/PSS and the PM IRRAS results obtained in this work for PAH-OsCN/PAA requires further experimental work. This discrepancy could arise from differences in thickness (the multilayers employed in this work have nine layers, while in SNIFTIRS experiments 29 layers were used) or in the relative hydrofobicity of the multilayers (both PAH-Os and PSS are expected to be more hydrophobic than PAH-OsCN and PAA, respectively).

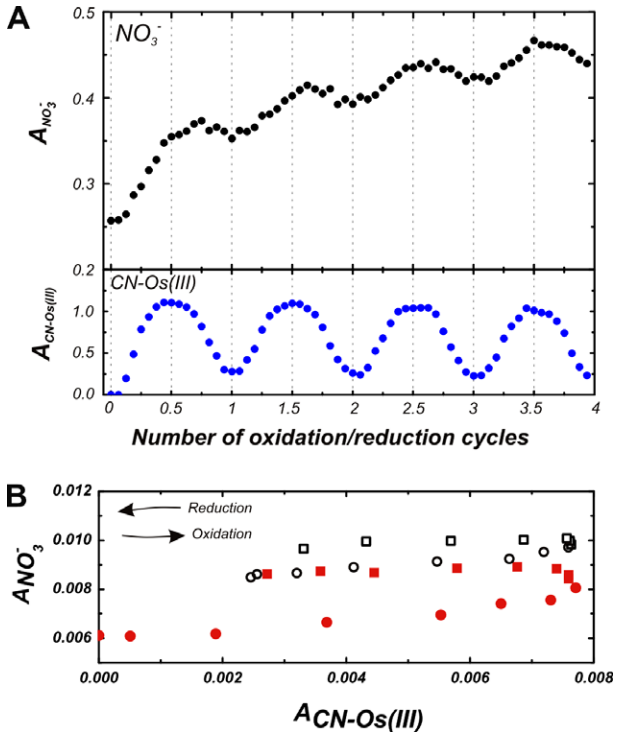

Fig. 9. A. Integrated peak area of the NO_3^- and CN—Os(III) bands for a freshly prepared $(PAH\text{-}OsCN/PAA)_4PAH\text{-}OsCN$ electrode in the experimental conditions of Fig. 8 showing four consecutive oxidation-reduction cycles. B. Nitrate peak area vs. CN—Os(III) peak area for the first (solid symbols) and second (open symbols) oxidation (circles)–reduction (squares) cycles.

4. Conclusions

We have shown that PM IRRAS spectroscopy can be used to study in situ the inner composition and environment of redox active LbL films. For the system PAH-OsCN/PAA, the technique provides direct information on the oxidation state of the pentacyano redox couple, the fraction of protonated carboxylates, the content of counterions and the film hydratation as a function of electrode potential and bulk solution composition. The novel redox polymer synthesized in this work allowed us to follow the oxidation state of the film. The stability towards ligand exchange of

the $[Os(CN)_5pyX]^{3-/2-}$ complex covalently attached to the polymer backbone is crucial in these experiments since long integration times are required for the FTIR spectroscopy of molecularly thin films (minutes to tens of minutes per spectrum). The high stability of the redox polymer was demonstrated by the negligible loss of its IR signal during several consecutive oxidation-reduction cycles.

This work demonstrates the simultaneous determination of the oxidation state and counterion content of an LbL film. Comparison of the potential evolution of the NO_3^- IR peak and the CN–Os(III) stretching band provided a spectroscopic, chemically specific proof of previous experimental observations. We proposed that nitrate is accumulated in the film mainly due to the incorporation of cations. This mechanism implies a loss of permselectivity probably due to the rupture of intrinsic polycation–polyanion pairs.

An interesting finding of the present work is that while approximately two thirds of the redox sites are electrically connected to the electrode and follow the Nernst relationship, the rest are electrochemically isolated. In a related work, it has been previously demonstrated by a combination of EQCM and electrochemical measurements that only a small fraction of the glucose oxidase (GOx) enzymes in LbL amperometric biosensors is electrically wired to the electrode [62]. Different authors have previously claimed complete or incomplete wiring of the redox polymers to the electrode for LbL electroactive films based on different experimental methods. We demonstrated that PM IRRAS provides unique spectroscopic information about electrical connectivity which cannot be gained through differential spectroelectrochemical techniques such as SNIFTIRS. Better understanding of the connectivity of polyelectrolyte modified electrodes is particularly important for the design of electrochemical devices such as biosensors, where an optimal use of the electroactive material is desirable and this publication is a further advance in this field.

Acknowledgment

E.J.C. acknowledges Fundacion Antorchas (Argentina) for a collaboration grant with Prof. Jacek Lipkowski of Guelph University (Canada) that allowed us to set up the PM IRRAS technique in Buenos Aires. Financial support from Universidad de Buenos Aires and CONICET is also acknowledged.

V.Z. would like to acknowledge the National Research and Engineering Council of Canada (NSERC) and Canadian Foundation for Innovation (CFI) as well as Fundación Antorchas (Argentina) for assistance in travel and accommodation during a collaborative visit to Argentina.

The authors would like to thank Nestor J. Filiel for the synthesis of PAH-OsCN and Prof. Federico Williams for the use of the XPS spectrometer. Enlightening discussions with Prof. Alejandro Parise on the synthesis of osmium complexes are also gratefully acknowledged.

References

[1] M. Osawa, in: R.C. Alkire, D.M. Kolb, J. Lipkowski, P.N. Ross (Eds.), Advances in Electrochemical Science and Engineering, Diffraction and Spectroscopic Methods in Electrochemistry, vol. 9, Wiley-VCH, Weinheim, 2009.
[2] V. Zamlynny, J. Lipkowski, in: R.C. Alkire, D.M. Kolb, J. Lipkowski, P.N. Ross (Eds.), Advances in Electrochemical Science and Engineering, Diffraction and Spectroscopic Methods in Electrochemistry, vol. 9, Wiley-VCH, Weinheim, 2009.
[3] B.L. Frey, R.M. Corn, S.C. Weibel, Polarization-Modulation Approaches to Reflection–Absorption Spectroscopy, Handbook of Vibrational Spectroscopy, vol. 2, John Wiley & Sons, 2001, p. 1042.
[4] J. Leitch, J. Kunze, J.D. Goddard, A.L. Schwan, R.J. Faragher, R. Naumann, W. Knoll, J.R. Dutcher, J. Lipkowski, Langmuir 25 (2009) 10354.
[5] C.L. Brosseau, X. Bin, S.G. Roscoe, J. Lipkowski, Journal of Electroanalytical Chemistry 621 (2008) 222.
[6] C.L. Brosseau, J. Leitch, X. Bin, M. Chen, S.G. Roscoe, J. Lipkowski, Langmuir 24 (2008) 13058.
[7] D. Matyszewska, J. Leitch, R. Bilewicz, J. Lipkowski, Langmuir 24 (2008) 7408.
[8] V. Zamlynny, I. Zawisza, J. Lipkowski, Langmuir 19 (2003) 132.
[9] G. Decher, B.J. Schlenoff, Multilayer Thin Films, Wiley-VCH, Weinheim, 2003.
[10] K. Itano, J. Choi, M.F. Rubner, Macromolecules 38 (2005) 3450.
[11] M. Tagliazucchi, D. Grumelli, E.J. Calvo, Physical Chemistry Chemical Physics 8 (2006) 5086.
[12] T.R. Farhat, J.B. Schlenoff, Journal of the American Chemical Society 125 (2003) 4627.
[13] J.A. Jaber, J.B. Schlenoff, Journal of the American Chemical Society 128 (2006) 2940.
[14] J.B. Schlenoff, A.H. Rmaile, C.B. Bucur, Journal of the American Chemical Society 130 (2008) 13589.
[15] J. Choi, M.F. Rubner, Macromolecules 38 (2005) 116.
[16] A.F. Xie, S. Granick, Journal of the American Chemical Society 123 (2001) 3175.
[17] A.F. Xie, S. Granick, Macromolecules 35 (2002) 1805.
[18] M. Tagliazucchi, E.J. Calvo, in: R.C. Alkire, D.M. Kolb, J. Lipkowski, P. Ross (Eds.), Chemically Modified Electrodes, Wiley-VCH, Weinheim, 2009.
[19] D.E. Grumelli, F. Garay, C.A. Barbero, E.J. Calvo, Journal of Physical Chemistry B 110 (2006) 15345.
[20] J.B. Schlenoff, H. Ly, M. Li, Journal of the American Chemical Society 120 (1998) 7626.
[21] D. Grumelli, C. Bonazzola, E.J. Calvo, Electrochemistry Communications 8 (2006) 1353.
[22] M. Tagliazucchi, D. Grumelli, C. Bonazzola, E.J. Calvo, Journal of Nanoscience and Nanotechnology 6 (2006) 1731.
[23] M. Tagliazucchi, E.J. Calvo, I. Szleifer, Langmuir 24 (2008) 2869.
[24] C. Bonazzola, E.J. Calvo, F.C. Nart, Langmuir 19 (2003) 5279.
[25] L.D. Slep, L.M. Baraldo, J.A. Olabe, Inorganic Chemistry 35 (1996) 6327.
[26] E.J. Calvo, R. Etchenique, C. Danilowicz, L. Diaz, Analytical Chemistry 68 (1996) 4186.
[27] L.M. Baraldo, M.S. Bessega, G.E. Rigotti, J.A. Olabe, Inorganic Chemistry 33 (1994) 5890.
[28] L.D. Slep, P. Alborés, L.M. Baraldo, J.A. Olabe, Inorganic Chemistry 41 (2002) 114.
[29] M. Tagliazucchi, F.J. Williams, E.J. Calvo, Journal of Physical Chemistry B 111 (2007) 8105.
[30] T. Buffeteau, B. Desbat, D. Blaudez, J.M. Turlet, Applied Spectroscopy 54 (2000) 1646.
[31] H.O. Finklea, D.A. Snider, J. Fedyk, Langmuir 6 (1990) 371.
[32] R.M.A. Azzam, N.M. Bashara, Ellipsometry and Polarized Light, North Holland Publishing Company, Amsterdam, 1977.
[33] F.M. Crean, K. Schug, Inorganic Chemistry 23 (1984) 853.
[34] K. Shigehara, N. Oyama, F.C. Anson, Journal of the American Chemical Society 103 (1981) 2552.
[35] M.E. Tagliazucchi, E.J. Calvo, Journal of Electroanalytical Chemistry 599 (2007) 249.
[36] E. Laviron, Journal of Electroanalytical Chemistry 112 (1980) 1.
[37] E.J. Calvo, A. Wolosiuk, Journal of the American Chemical Society 124 (2002) 8490.
[38] V. Flexer, E.S. Forzani, E.J. Calvo, S.J. Ludueña, L.I. Pietrasanta, Analytical Chemistry 78 (2006) 399.
[39] P. Albores, L.D. Slep, L.M. Baraldo, R. Baggio, M.T. Garland, E. Rentschler, Inorganic Chemistry 45 (2006) 2361.
[40] D. Lin-Vien, N.B. Colthup, W.G. Fateley, J.G. Graselli, The Handbook of Infrared and Raman Characteristic Frequencies of Organic Molecules, Academic Press, New York, 1991.
[41] J.J. Harris, P.M. DeRose, M.L. Bruening, Journal of the American Chemical Society 121 (1999) 1978.
[42] L. Wang, Y. Fu, Z. Wang, Y. Fan, X. Zhang, Langmuir 15 (1999) 1360.
[43] A.I. Petrov, A.A. Antipov, G.B. Sukhorukov, Macromolecules 36 (2003) 10079.
[44] S.E. Burke, C.J. Barrett, Langmuir 19 (2003) 3297.
[45] K. Nakamoto, Infrared and Raman Spectra of Inorganic and Coordination Compounds, John Wiley & Sons, New York, 1986.
[46] N.S. Marinković, J.J. Calvente, A. Kloss, Z. Kováčová, W, Ronald Fawcett, Journal of Electroanalytical Chemistry 467 (1999) 325.
[47] D. Blaudez, T. Buffeteau, J.C. Cornut, B. Desbat, N. Escafre, M. Pezolet, J.M. Turlet, Thin Solid Films 242 (1994) 146.
[48] S. Giasson, T. Palermo, T. Buffeteau, B. Desbat, J.M. Turlet, Thin Solid Films 252 (1994) 111.
[49] I. Pelletier, H. Bourque, T. Buffeteau, D. Blaudez, B. Desbat, M. Pézolet, Journal of Physical Chemistry B 106 (2002) 1968.
[50] I. Zawisza, J. Lipkowski, Langmuir 20 (2004) 4579.
[51] Y. Cheng, R.M. Corn, Journal of Physical Chemistry B 103 (1999) 8726.
[52] C. Combellas, F. Kanoufi, S. Sanjuan, C. Slim, Y. Tran, Langmuir 25 (2009) 5360.
[53] D.N. Blauch, J.-M. Savéant, Journal of the American Chemical Society 114 (1992) 3323.
[54] A.R. Hillman, Solid State Ionics 94 (1997) 151.
[55] H. Sato, J-i. Anzai, Biomacromolecules 7 (2006) 2072.
[56] A. Liu, J. Anzai, Langmuir 19 (2003) 4043.
[57] D. Laurent, J.B. Schlenoff, Langmuir 13 (1997) 1552.
[58] T. Fushimi, A. Oda, H. Ohkita, S. Ito, Thin Solid Films 484 (2005) 318.
[59] N. Tognalli, A. Fainstein, C. Bonazzola, E. Calvo, Journal of Chemical Physics 120 (2004) 1905.
[60] M. Adusumilli, M.L. Bruening, Langmuir 25 (2009) 7478.
[61] C. Barbero, Physical Chemistry Chemical Physics 7 (2005) 1885.
[62] J. Hodak, R. Etchenique, E.J. Calvo, K. Singhal, P.N. Bartlett, Langmuir 13 (1997) 2708.